# Universality of the energy-containing structures in wall-bounded turbulence

**Charitha M. de Silva**[1,†], **Dominik Krug**[1], **Detlef Lohse**[2,3]
**and Ivan Marusic**[1]

[1]Department of Mechanical Engineering, University of Melbourne, Victoria 3010, Australia

[2]Physics of Fluids Group and Twente Max Planck Center, Department of Science and Technology, Mesa+ Institute, and J.M. Burgers Center for Fluid Dynamics, University of Twente, PO Box 217, 7500 AE Enschede, The Netherlands

[3]Max Planck Institute for Dynamics and Self-Organization, 37077 Göttingen, Germany

The scaling behaviour of the longitudinal velocity structure functions $\langle (\Delta_r u)^{2p} \rangle^{1/p}$ (where $2p$ represents the order) is studied for various wall-bounded turbulent flows. It has been known that for very large Reynolds numbers within the logarithmic region, the structure functions can be described by $\langle (\Delta_r u)^{2p} \rangle^{1/p}/U_\tau^2 \approx D_p \ln(r/z) + E_p$ (where $r$ is the longitudinal distance, $z$ the distance from the wall, $U_\tau$ the friction velocity and $D_p$, $E_p$ are constants) in accordance with Townsend's attached eddy hypothesis. Here we show that the ratios $D_p/D_1$ extracted from plots between structure functions – in the spirit of the extended self-similarity hypothesis – have further reaching universality for the energy containing range of scales. Specifically, we confirm that this description is universal across wall-bounded flows with different flow geometries, and also for both the longitudinal and transversal structure functions, where previously the scaling has been either difficult to discern or differences have been reported when examining the direct representation of $\langle (\Delta_r u)^{2p} \rangle^{1/p}$. In addition, we present evidence of this universality at much lower Reynolds numbers, which opens up avenues to examine structure functions that are not readily available from high Reynolds number databases.

**Key words:** turbulent boundary layers, turbulent flows

## 1. Introduction

Developed turbulence is characterized by its non-Gaussian, intermittent statistics at the small scales (Frisch 1995; Pope 2000). The universality of these statistics was established about two decades ago (Arneodo *et al.* 1996; Belin, Tabeling & Willaime 1996) by employing the so-called extended self-similarity (ESS) hypothesis (Benzi *et al.* 1993, 1995). That is, rather than focusing on the scaling of the $n$th-order streamwise velocity ($u$) structure function for the inertial subrange (ISR) scales, which scales as

$$\langle [u(\boldsymbol{x} + \boldsymbol{i}r) - u(\boldsymbol{x})]^n \rangle \propto r^{\xi_n}, \tag{1.1}$$

† Email address for correspondence: desilvac@unimelb.edu.au

where $r$ represents the spatial separation, $\zeta_n$ the scaling exponents, $i$ an unit vector in the streamwise direction and $\langle \rangle$ indicates averaged quantities, the focus is on the relative scaling of one structure function with respect to another. Traditionally, scaling is computed relative to the third-order structure function $\langle |\Delta u_r|^3 \rangle$ of the modulus of the velocity difference, following

$$\langle (\Delta_r u)^n \rangle \propto \langle |\Delta_r u|^3 \rangle^{\xi_n}. \tag{1.2}$$

The intermittency exponents $\xi_n$ show a universal non-Kolmogorov K41 dependence (i.e. $\xi_n \neq n/3$) on $n$, which can be characterized by the She–Leveque hierarchies (She & Leveque 1994) or the $p$-model of Meneveau & Sreenivasan (1987). To conform with recent work on even moments (Meneveau & Marusic 2013; de Silva *et al.* 2015), we shall set $n = 2p$ below, and define the normalized dimensionless longitudinal structure function as $\langle (\Delta_r u_+)^{2p} \rangle^{1/p}$. Here, the velocity and length scales are given in viscous/wall units, and are denoted by the subscript/superscript $+$. For example, we use $l^+ = lU_\tau/\nu$ for length and $u^+ = u/U_\tau$ for velocity, where $U_\tau$ is the mean friction velocity and $\nu$ is the kinematic viscosity of the fluid.

The universality for the ISR scaling properties in ESS form following (1.2) has been shown to hold for various flow types and even down to very small Taylor–Reynolds numbers ($Re_\lambda \approx 100$) (Grossmann, Lohse & Reeh 1997*a*,*b*), even though universality might not be easily discernible from the structure functions, $\langle (\Delta_r u_+)^{2p} \rangle^{1/p}$, themselves. However, in wall turbulence this universality has been thought to break down on the large, so-called energy-containing range (ECR), scales (Pope 2000), where the wall boundedness and the different geometric features of the flow boundary conditions should play an increasingly important role.

In this work, a further reaching universality for the scaling behaviour of the ECR scales in wall-bounded turbulence is explored. Accordingly, we focus – in the spirit of ESS – on the relative relations of the velocity structure functions in the ECR scales across both a wide range of wall-bounded flow geometries and Reynolds numbers.

The increasing popularity of Townsend's attached eddy hypothesis (Townsend 1976; Perry, Henbest & Chong 1986; Meneveau & Marusic 2013; Yang, Marusic & Meneveau 2016*a*) has revealed new insight into the universality of the ECR scales, $z < r \ll \delta$ (where $z$ and $\delta$ corresponds to the wall-normal distance and boundary layer thickness, respectively), in wall-bounded turbulence. Recently, de Silva *et al.* (2015) examined turbulent boundary layers at friction Reynolds numbers, $Re_\tau = \delta U_\tau/\nu$, of order $10^4$. Their work confirmed that at sufficiently high Reynolds numbers the ECR scales of the normalized even-ordered longitudinal structure functions can be described by

$$\langle (\Delta_r u_+)^{2p} \rangle^{1/p} = D_p \ln\left(\frac{r}{z}\right) + E_p, \tag{1.3}$$

where $r$ is the longitudinal distance, $z$ the distance from the wall and $D_p$, $E_p$ are constants. Such a representation is shown in figure 1(*a*), which presents the longitudinal second-order structure function, $\langle (\Delta_r u_+)^2 \rangle$, from the boundary layer databases used in the present work (see table 1 for further details). Results from each database are computed at approximately the geometric centre of the logarithmic region, which is taken to nominally span the range $3\sqrt{Re_\tau} < z^+ < 0.15 Re_\tau$ (Marusic *et al.* 2013). The solid line in figure 1(*a*,*b*) reproduces the scaling described by (1.3) with the coefficients reported by de Silva *et al.* (2015). The results exhibit good agreement in the ECR scales ($z < r \ll \delta$) for the high Reynolds number databases.
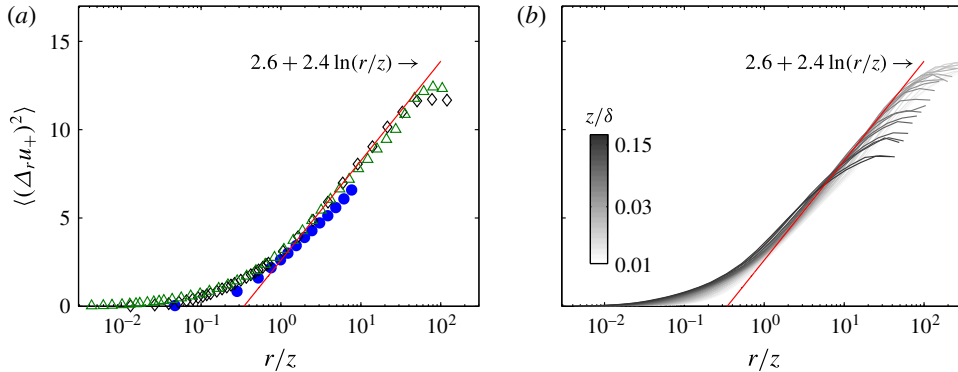
FIGURE 1. (Colour online) (*a*) The second-order longitudinal structure function, $\langle(\Delta_r u_+)^2\rangle$ versus $r/z$. The symbols represent different datasets (defined in table 1), and the results are computed at wall-normal locations within the logarithmic region: $\diamond$: $z^+ \approx 800$, $\triangle$: $z^+ \approx 1.6 \times 10^4$ and $\bullet$: $z^+ \approx 150$. (*b*) $\langle(\Delta_r u_+)^2\rangle$ versus $r/z$ at $Re_\tau \approx 19\,000$ ($\diamond$ symbols) across the range $0.01 < z/\delta < 0.15$. The solid line (——) in (*a,b*) corresponds to a log-law fit following (1.3) in the range $z < r \ll \delta$.

However, even at Reynolds numbers in excess of $O(10^4)$, scaling is only present over less than a decade of $r/z$.

Further, to illustrate the influence of the wall-normal position, $z$, figure 1(*b*) shows $\langle(\Delta_r u_+)^2\rangle$ computed for the database at $Re_\tau \approx 19\,000$ at different $z$ within the logarithmic region. Here, it is evident that the extent of scales (following (1.3)) is impacted by the chosen $z$, with an earlier peel-off from (1.3) with increasing $z$, consistent with the scaling range $z < r \ll \delta$ (Davidson, Nickels & Krogstad 2006). Additionally, this log-law scaling is even harder to discern at $Re_\tau \sim O(10^3)$ for the ECR scales (to be discussed further in § 4.1), as these flows are yet to exhibit a clear logarithmic region in the variance (Smits, McKeon & Marusic 2011). However, direct numerical simulation (DNS) databases at $Re_\tau \sim O(10^3)$ have access to volumetric, multi-component information. Therefore, if one can discern the scaling for the ECR scales from these databases it would open avenues to examine the other velocity components/directions. In this work, we will show that the universality of the scaling for the ECR scales in an ESS framework is applicable to $Re_\tau \sim O(10^3)$ as well as different flow geometries of wall-bounded turbulence. Previous studies (see Chung *et al.* (2015) for pipe flows and Sillero, Jiménez & Moser (2013) for channel flows) have reported that the scaling behaviour of the ECR scales differs, based on flow geometry if one is restricted to a classical analysis.

Throughout this paper, the coordinate system $x$, $y$ and $z$ refers to the streamwise, spanwise and wall-normal directions, respectively. The corresponding instantaneous streamwise, spanwise and wall-normal velocity fluctuations are represented by $u$, $v$ and $w$.

## 2. Experimental and numerical databases

This study utilizes a collection of wall-bounded flow databases from both experimental and numerical works, which are summarized in table 1. Collectively, they cover different flow geometries (boundary layer, channel and pipe flow) and span a wide range of Reynolds numbers.

| Symbol | Flow | Reference | Technique | $\approx Re_\tau$ |
|---|---|---|---|---|
| ◇ | Boundary layer | Hutchins *et al.* (2009) | Hot-wire | 19 000 |
| △ | Atmospheric Bound. layer | Kunkel & Marusic (2006) | Hot-wire | $3 \times 10^6$ |
| ●, ▶ | Boundary layer | Sillero *et al.* (2013) | DNS | 1600 |
| ◀ | Channel flow | del Alamo *et al.* (2004) | DNS | 930 |
| □ | Pipe flow | Ng *et al.* (2011) | Hot-wire | 3000 |

TABLE 1. Summary of experimental and numerical databases and their corresponding symbols. Databases with two symbols have access to both longitudinal and transversal information.

The high *Re* laboratory boundary layer dataset (◇ symbols) is acquired from the High Reynolds Number Boundary Layer Wind Tunnel (HRNBLWT) at the University of Melbourne. Further details of the facility are provided in Nickels *et al.* (2005). The measurement is obtained using hotwire anemometry using a 2.5 µm diameter Wollaston wire operated by an in-house constant-temperature anemometer. We note that this and all other databases used in the present work are acquired with a spatial resolution sufficient to resolve the turbulence intensity accurately within the logarithmic region based on the guidelines laid out by Hutchins *et al.* (2009). The highest *Re* database (△ symbols) is acquired from the atmospheric boundary layer at the surface layer turbulence and environmental test facility (SLTEST) located in the Utah salt flats (Kunkel & Marusic 2006) again employing hot-wires positioned within the logarithmic region.

To compliment the high *Re* databases from boundary layers, we include a recent numerical database of a turbulent boundary layer at $Re_\tau \approx 1600$ (Sillero *et al.* 2013). For the present study, we use seven volumetric fields with a streamwise and spanwise extent of approximately $1\delta$ and $10\delta$, respectively, thus allowing us to compute both the longitudinal (● symbols) and transversal (▶ symbols) structure functions. The final two databases are from a channel flow DNS by del Alamo *et al.* (2004) and a pipe flow measurement by Ng *et al.* (2011). Similar to the boundary layer case, we use five volumetric fields with a streamwise and spanwise extent of $8\pi\delta$ and $3\pi\delta$, respectively, for the channel flow DNS. The pipe flow measurement is acquired using hot-wire anemometry in a similar fashion to the high *Re* boundary layer databases. Further details on all measurements can be found in their respective publications. We note for all the hot-wire anemometry database we use Taylor's frozen turbulence hypothesis to convert the time-series information from the hot-wires to spatial information using the local mean velocity as the convection velocity. The validity of using Taylor's frozen turbulence hypothesis at least up to $r < \delta$ is confirmed by de Silva *et al.* (2015). Other studies which have also assessed the accuracy of invoking Taylor's hypothesis include Dennis & Nickels (2008), Del Alamo & Jiménez (2009), Chung & McKeon (2010), Atkinson, Buchmann & Soria (2014).

The subsequent analysis involves computing higher-order moments, therefore a brief discussion on the degree of convergence of the higher moments is warranted. The convergence of the hot-wire databases (◇, △ and □ symbols) has already been established by de Silva *et al.* (2015) up to $p = 5$ or the tenth-order moment. Meanwhile, for the DNS databases, we are limited by the number of accessible volumes, therefore the premultiplied probability density function for velocity fluctuations $(\Delta_r u_+)^{2p} P(\Delta_r u^+)$ is computed in order to assess the degree of convergence following the approach described in Meneveau & Marusic (2013) and Huisman, Lohse
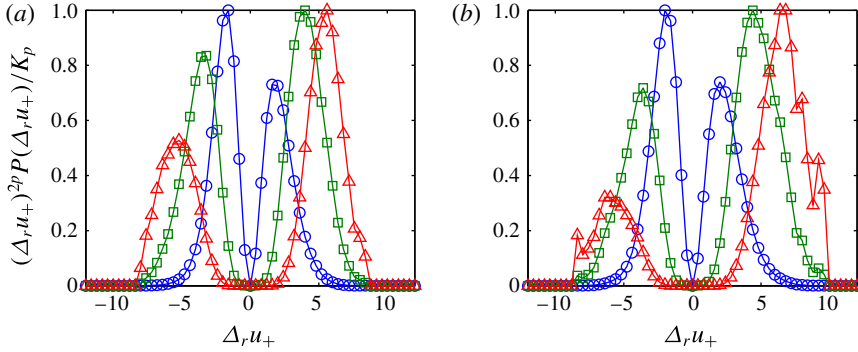
FIGURE 2. (Colour online) Premultiplied probability density function of $\Delta_r u_+$ at $r \approx z^+$ within the logarithmic region. $(a,b)$ Correspond to the boundary layer DNS of Sillero *et al.* (2013) and the channel flow DNS of del Alamo *et al.* (2004), respectively. The moments $2p = 2$, 6, and 10 are represented by $\bigcirc$, $\square$ and $\triangle$, respectively. Curves are divided by an arbitrary factor $K_p$ such that the maximum for all orders is one.

& Sun (2013). The results are shown in figure 2 for the two DNS databases and reveal that acceptable convergence is observed up to $2p = 6$ in the sense that the respective structure function of order $2p$, which is the area under the curve, is captured well (i.e. the tails of the distributions plotted in figure 2 are smooth). However, convergence at $2p = 8$ and beyond is moderate, therefore, for the subsequent analysis results from the DNS datasets at $2p > 6$ should be considered with due caution.

## 3. Relative relations of structure functions for the ECR scales

Based on our observations from the streamwise structure function for the ECR scales in turbulent boundary layers (see figure 1) it is evident that (1.3) holds over a very limited range of scales, even for high *Re* flows of $O(10^4)$. Therefore, in order to establish further reaching universality, we examine – in the spirit of ESS – the relative relations of the velocity structure functions. That is, rather than examining $\langle (\Delta_r u_+)^{2p} \rangle^{1/p}$ versus $\log(r/z)$ as in figure 1, we plot $\langle (\Delta_r u_+)^{2p} \rangle^{1/p}$ versus $\langle (\Delta_r u_+)^{2m} \rangle^{1/m}$, thus obtaining the ratios $D_p/D_m$ of the coefficients $D_p$ from the slopes of such plots. Specifically, for the ECR scales following (1.3) we obtain the ratios

$$\langle (\Delta_r u_+)^{2p} \rangle^{1/p} = \frac{D_p}{D_m} \langle (\Delta_r u_+)^{2m} \rangle^{1/m} + E_p - \frac{D_p}{D_m} E_m. \tag{3.1}$$

In figure 3($a$) we show this type of plot for $\langle (\Delta_r u_+)^4 \rangle^{1/2}$ versus $\langle (\Delta_r u_+)^2 \rangle$. Compared to the direct representation, $\langle (\Delta_r u_+)^{2p} \rangle^{1/p}$ versus $\log(r/z)$ (cf. figure 1$a$), which was limited to the range $z < r \ll \delta$, the results reveal a convincingly extended scaling range beyond $r \gtrsim z$. Further, an accurate estimate of $D_p/D_m$ can now also be obtained from the lower *Re* database at $Re_\tau \approx 1600$, highlighting the extended universality of (3.1) for the ECR scales. This in turn would allow us to discern the scaling coefficients of structure functions from other velocity components/directions, which are more readily accessible from databases at $Re_\tau \sim O(10^3)$. It is worth noting that if the distribution of $\Delta_r u$ was Gaussian, the scaling ratios would be known, i.e. then $\langle (\Delta_r u_+)^{2p} \rangle^{1/p} = [(2p - 1)!!]^{1/p} \langle (\Delta_r u_+)^2 \rangle$. However, in the general case such a simple relation does not exist. Therefore, since $\Delta_r u$ is non-Gaussian (i.e. non-zero third moment, non-zero
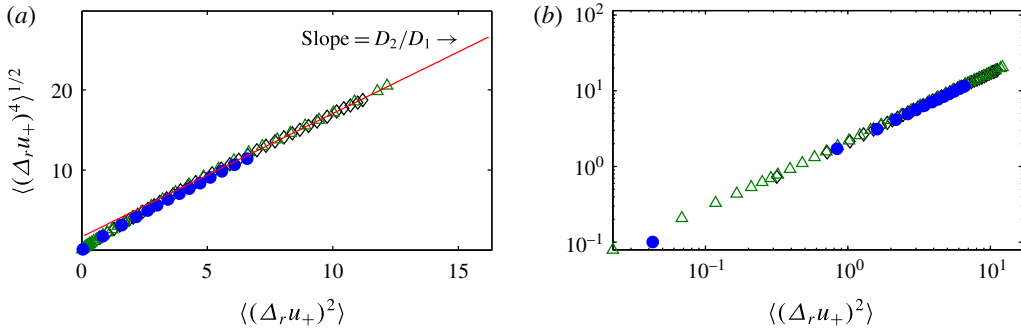
FIGURE 3. (Colour online) (*a*) ESS plot for $\langle(\Delta_r u_+)^4\rangle^{1/2}$ versus $\langle(\Delta_r u_+)^2\rangle$. The symbols represent different datasets (defined in table 1), and the results are computed at wall-normal locations within the logarithmic region: $\diamond$: $z^+ \approx 800$, $\triangle$: $z^+ \approx 1.6 \times 10^4$ and $\bullet$: $z^+ \approx 150$. The solid line (——) corresponds to a fit following (3.1) to the experimental database at $Re_\tau \approx 19\,000$. For reference (*b*) shows (*a*) reproduced on a log–log plot in the traditional ESS form between $\langle(\Delta_r u_+)^4\rangle^{1/2}$ and $\langle(\Delta_r u_+)^2\rangle$.

additive constant $[E_p - (D_p/D_m)E_m]$ in (3.1), see also de Silva *et al.* (2015)), the scaling described in (3.1) is a non-trivial result.

As an aside, we also include the traditional ESS plot (cf. figure 3*b* for reference), where $\langle(\Delta_r u_+)^4\rangle^{1/2}$ and $\langle(\Delta_r u_+)^2\rangle$ are plotted on log–log scales. Benzi *et al.* (1993, 1995) have shown that in this form better estimates of the relative ISR scaling exponents, $\zeta_p/\zeta_m$, can be computed compared to the velocity structure function $\langle\Delta_r u_+^{2p}\rangle^{1/p} \propto r^{\zeta_{2p}/p}$ itself.

To further validate the improved robustness of the scaling described in (3.1) for the ECR scales, figure 4(*a–c*) presents results for the even, higher-order structure functions at approximately the geometric centre of the logarithmic region. The results show good collapse of the higher-order moments up to $2p = 10$ and provide further direct support for (3.1). To quantify these findings, figure 4(*d*) and table 2 present the ratios of $D_p$ relative to $D_m$ (with $m = 1$) computed based on a linear fit in the range $r \gtrsim z$. We note good agreement with the coefficients reported by de Silva *et al.* (2015) who had access to sufficiently high $Re$ databases, however, following (3.1) we can reproduce accurate estimates even for the low $Re$ databases ($\bullet$ symbols) in the present work. Previously, databases at comparably low $Re$ would only provide a poor direct estimate of $D_p$ following (1.3) (see also figure 6). Table 2 also presents estimates of the higher-order coefficients $D_{2-5}$ for reference from the database at $Re_\tau \approx 19\,000$, determined from the computed ratios $D_p/D_m$ (now over a much wider range of scales, $\sim r \gtrsim z$) together with a known estimate of one coefficient (here chosen to be $D_1$). It should be noted that computing higher-order moments, particularly from experimental databases, can be prone to inaccuracies due to the presence of measurement noise. Nevertheless, here we observe consistent support for (3.1) across a wide range of experimental databases and numerical databases.

# 4. Further evidence of universality

## 4.1. *Influence of wall-normal location and flow geometry*

Previously, it was highlighted that the scaling observed for the ECR scales is prevalent across a finite wall-normal extent (see figure 1). Specifically, even-order structure
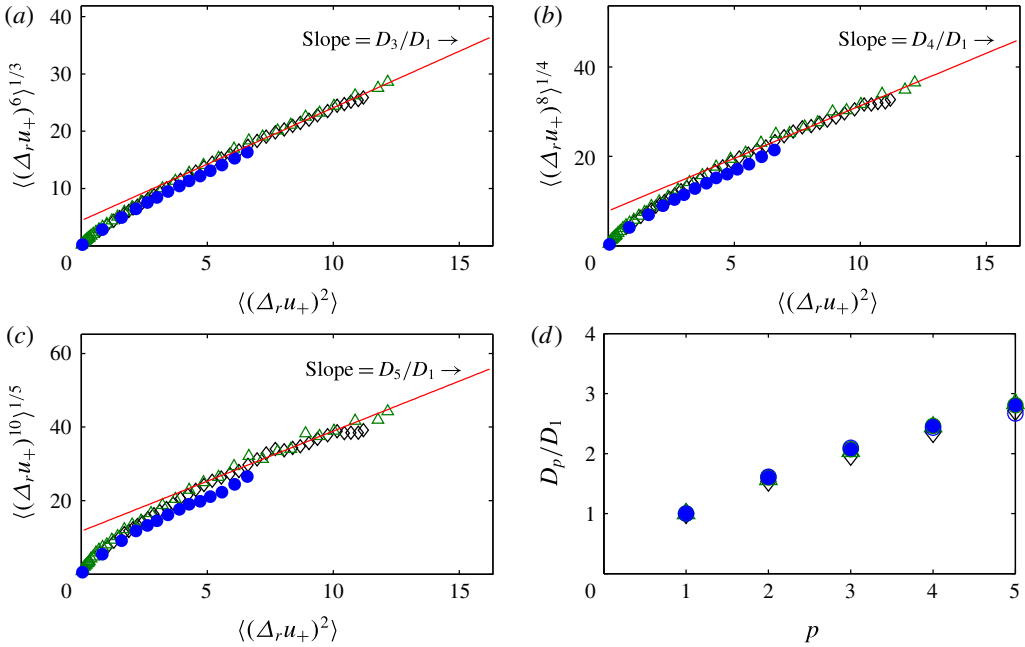
FIGURE 4. (Colour online) ESS plot for higher-order moments for the same databases shown in figure 3. (*a*) $\langle(\Delta_r u_+)^6\rangle^{1/3}$ versus $\langle(\Delta_r u_+)^2\rangle$, (*b*) $\langle(\Delta_r u_+)^8\rangle^{1/4}$ versus $\langle(\Delta_r u_+)^2\rangle$ and (*c*) $\langle(\Delta_r u_+)^{10}\rangle^{1/5}$ versus $\langle(\Delta_r u_+)^2\rangle$. The solid red lines (——) correspond to a fit following (3.1) to the experimental database at $Re_\tau \approx 19\,000$, and the values $D_p/D_1$ are tabulated in table 2. (*d*) Ratios $D_p/D_1$ for the different databases. The symbols in all panels represent different datasets (defined in table 1), and the results are computed at wall-normal locations within the logarithmic region: $\diamondsuit$: $z^+ \approx 800$, $\triangle$: $z^+ \approx 1.6 \times 10^4$ and $\bullet$: $z^+ \approx 150$.

| | SLTEST – hot-wire $Re_\tau \approx 3 \times 10^6$ $z^+ \approx 1.6 \times 10^4$ | Bound. layer – DNS $Re_\tau \approx 1600$ $z^+ \approx 150$ | HRNBLWT – hot-wire $Re_\tau \approx 19\,000$ $z^+ \approx 800$ | |
|---|---|---|---|---|
| | $D_p/D_1$ | $D_p/D_1$ | $D_p/D_1$ | $D_p$ |
| $p = 1$ | 1.00 | 1.00 | 1.00 | *2.45 |
| $p = 2$ | $1.56 \pm 0.02$ | $1.63 \pm 0.01$ | $1.53 \pm 0.01$ | 3.76 |
| $p = 3$ | $2.04 \pm 0.05$ | $2.14 \pm 0.02$ | $1.97 \pm 0.03$ | 4.82 |
| $p = 4$ | $2.45 \pm 0.09$ | $2.53 \pm 0.05$ | $2.35 \pm 0.07$ | 5.74 |
| $p = 5$ | $2.83 \pm 0.16$ | $2.80 \pm 0.10$ | $2.71 \pm 0.16$ | 6.65 |

TABLE 2. Comparison of the ratios $D_p/D_1$ for the ECR scales from different turbulent boundary layer datasets. The range for each $D_p/D_1$ estimate indicates a 95 % confidence bound. The scaling constants, $D_p$, is presented at $Re_\tau \approx 19\,000$ based on the reference value, $D_1$ (indicated by the * symbol) from the same database.

functions are reported to follow (1.3) within the bounds of the logarithmic region (Davidson *et al.* 2006), where self-similarity is most prevalent as bulk flow effects $[z \sim O(\delta)]$ or viscous effects $[z^+ \sim O(1)]$ are minimal. Recent work on moment generating functions by Yang *et al.* (2016*b*) has shown that the extent of logarithmic
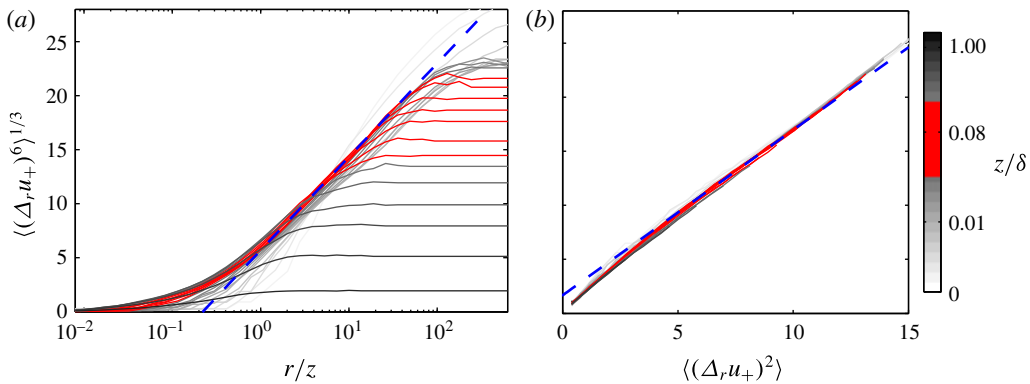
FIGURE 5. (Colour online) (*a*) $\langle (\Delta_r u_+)^6 \rangle^{1/3}$ versus $r/z$ at all available wall-normal (*z*) locations from the hot-wire dataset of Hutchins *et al.* (2009) at $Re_\tau \approx 19\,000$. Each line corresponds to different *z* locations from the wall up to $z/\delta \approx 1$ with darker shading corresponding to higher *z*. The red lines (——) highlight *z* locations within the logarithmic region. The blue dashed line (– –) corresponds to the scaling law expected for the ECR scales. (*b*) Shows (*a*) reproduced now as a relation between $\langle (\Delta_r u_+)^6 \rangle^{1/3}$ and $\langle (\Delta_r u_+)^2 \rangle$, revealing universality.

scaling as a function of *z* increases when examining ratios between moment generating functions in ESS form. They postulated that bulk flow or viscous effects would affect all moment generating functions similarly, therefore, their ratio would exhibit a larger self-similarity region. Here, we explore if the structure functions also exhibit similar behaviour at the ECR scales, with an extended wall-normal extent following (3.1).

To this end, figure 5(*a*) presents the sixth-order structure function, $\langle (\Delta_r u_+)^6 \rangle^{1/3}$, versus spatial separation *r* across the entire boundary layer for the dataset at $Re_\tau = 19\,000$. We note that the sixth-order structure function is chosen as a representative case to highlight any subtle differences as a function of wall-normal height, when plotted in the ESS framework. Each line corresponds to $\langle (\Delta_r u_+)^6 \rangle^{1/3}$ computed at a fixed wall-normal (*z*) location within the range $10 < z^+ < Re_\tau$. The results show that even at $Re_\tau \sim O(10^4)$ a log law for the ECR scales is only discernible within the logarithmic region, which are highlighted by the red lines (——). Figure 5(*b*) reproduces the same statistics across the entire boundary layer for $\langle (\Delta_r u_+)^6 \rangle^{1/3}$, but now as a function of $\langle (\Delta_r u_+)^2 \rangle$. The results exhibit encouraging collapse across a much larger wall-normal extent ($z^+ \gtrsim 50$) following (3.1) compared to directly examining $\langle (\Delta_r u_+)^6 \rangle^{1/3}$ versus spatial separation *r*. We note that beyond $z^+ \gtrsim 50$ the multiplicative constant, i.e. the ratio $D_p/D_1$, appears unchanged, while the additive constant in (3.1) has a subtle trend with *z*. In any case, in the ESS inspired framework, we are able to discern the scaling coefficients (slopes $D_p/D_1$) of the ECR scales more accurately, particularly at low Reynolds numbers when no clear logarithmic region exists.

Scaling of the ECR scales for different flow geometries in wall-bounded turbulence has been a subject of interest over the last decade (e.g. Monty *et al.* 2009). Most works have placed emphasis on examining the spectral energy distribution (Jiménez 2012). More recently, Chung *et al.* (2015) compared structure functions for pipe flow and boundary layers over a wide range of *Re* and highlighted a notably shallower slope, $D_1$, for pipe flows, which was less discernible for pipe flows with increasing *Re*. To highlight these differences due to flow geometry, figure 6(*a*) presents $\langle (\Delta_r u_+)^4 \rangle^{1/2}$
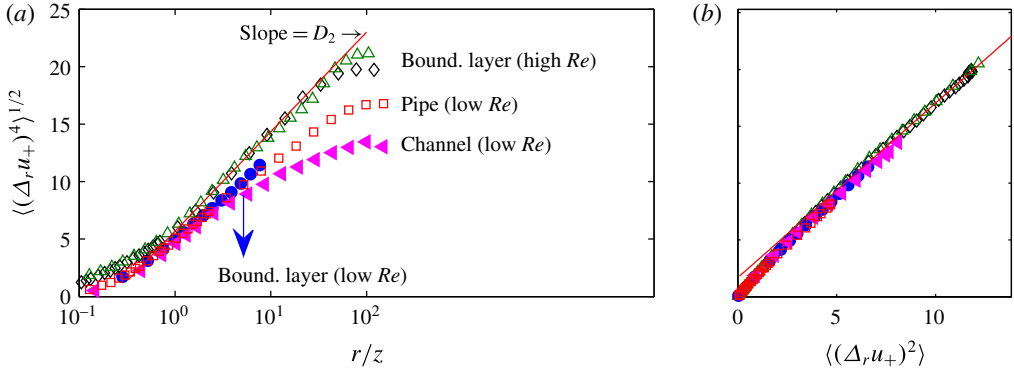
FIGURE 6. (Colour online) (*a*) $\langle(\Delta_r u_+)^4\rangle^{1/2}$ versus $r/z$ computed from boundary layers, pipes and channel flows at different $Re$. The symbols represent different datasets (defined in table 1), and the results are computed at wall-normal locations within the logarithmic region: $\diamondsuit$: $z^+ \approx 800$, $\triangle$: $z^+ \approx 1.6 \times 10^4$, $\bullet$: $z^+ \approx 150$, $\square$: $z^+ \approx 200$ and $\blacktriangleleft$: $z^+ \approx 110$. (*b*) $\langle(\Delta_r u_+)^4\rangle^{1/2}$ versus $\langle(\Delta_r u_+)^2\rangle$ for all the datasets shown in (*a*), again displaying enhanced universality as compared to (*a*). The solid red lines (——) in (*a*,*b*) corresponds to the scaling law expected for the ECR scales.

from pipes, channels and boundary layers. Results for the three flow geometries are presented at a comparable $Re_\tau$ ($\sim$1000–3000) and are computed at approximately the geometric centre of the logarithmic region. The results show clear evidence that the ECR scales exhibit different scaling behaviour indicating that the flow geometry does play a role. However, once plotted as a ratio between structure functions of different orders (see figure 6*b*), good collapse is observed across the three flow geometries considered in the present work. Hence, these findings show further reaching universality for the scaling of the ECR scales for different flow geometries in wall turbulence, even at $Re_\tau = O(10^3)$ when presented using an ESS inspired framework. Therefore, we postulate that even though the influence of geometrical effects (such as 'crowding' in pipe flows, Chung *et al.* 2015) is likely to exist in structure functions at different orders, we are still able to accurately quantify the scaling of the ratios between two structure functions ($D_p/D_m$) for the ECR scales. Moreover, if one has an accurate estimate of the scaling constants for $\langle(\Delta_r u_+)^2\rangle$, the behaviour of the higher-order counterparts, can be estimated using the ratios presented in table 2.

To further validate the improved robustness of the scaling described in (3.1) for the ECR scales over different flow geometries, figure 7(*a*,*b*) presents $\langle(\Delta_r u_+)^4\rangle^{1/2}$ as a function of $\langle(\Delta_r u_+)^2\rangle$ computed further away from the wall at $z \approx 0.15\delta$ and $z \approx 0.5\delta$, respectively. The results show good agreement between all the databases exhibiting universality beyond the logarithmic region. Furthermore, the slope of the scaling law ($D_2/D_1$) expected for the ECR scales (solid red line, ——) is nominally constant, albeit with a subtle shift in the additive constants, $E_p - (D_p/D_m)E_m$, in (3.1) with increasing $z$.

### 4.2. *Transversal structure functions in wall-bounded turbulence*

The preceding discussions have shown that by plotting the ratios between longitudinal structure functions of different orders further reaching universality can be achieved
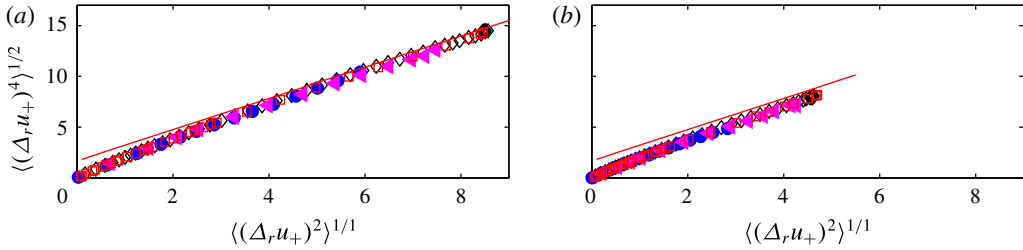
FIGURE 7. (Colour online) $(a,b)$ $\langle(\Delta_r u_+)^4\rangle^{1/2}$ versus $\langle(\Delta_r u_+)^2\rangle$ computed at $z \approx 0.15\delta$ and $z \approx 0.5\delta$, respectively. The symbols represent different datasets (defined in table 1). The solid red lines (——) in $(a,b)$ are identical and correspond to the scaling law estimated for the ECR scales following (3.1) in the logarithmic region.
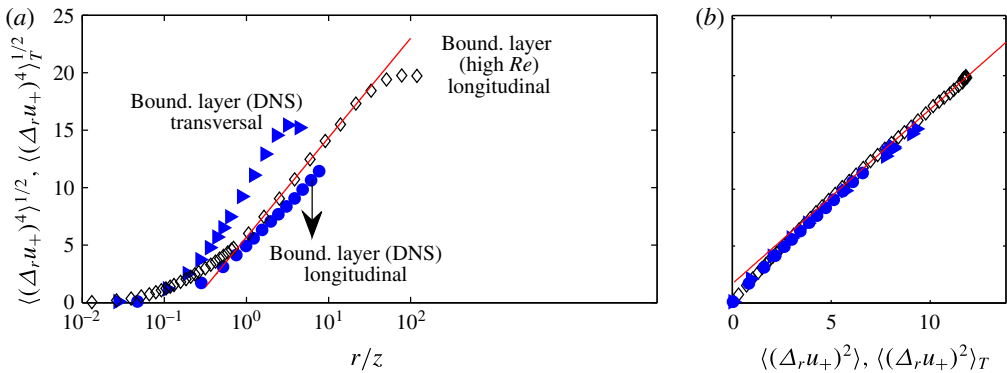


FIGURE 8. (Colour online) $(a)$ $\langle(\Delta_r u_+)^4\rangle^{1/2}$ versus $r/z$ computed from boundary layers in the longitudinal and transversal directions. The symbols represent different datasets (defined in table 1), and the results are computed at wall-normal locations within the logarithmic region: $\diamond$: $z^+ \approx 800$ and ▶, ●: $z^+ \approx 150$. $(b)$ The transversal and longitudinal structure functions as a function of their respective second-order structure functions, i.e. $\langle(\Delta_r u_+)^4\rangle^{1/2}$ versus $\langle(\Delta_r u_+)^2\rangle$ and $\langle(\Delta_r u_+)^4\rangle_T^{1/2}$ versus $\langle(\Delta_r u_+)^2\rangle_T$. The solid red lines (——) in $(a,b)$ corresponds to the scaling law expected for the ECR scales.

for the scaling behaviour of the ECR scales, now even at $Re_\tau = O(10^3)$. Therefore, it would be interesting to explore if this universality also extends to the transversal structure function at the ECR scales (see e.g. Grossmann *et al.* (1997*b*), van de Water & Herweijer (1999), Kurien *et al.* (2000), Jacob *et al.* (2004) for a discussion on the scaling for the ISR scales), which is more readily accessible at $Re_\tau = O(10^3)$ from numerical databases. Here the transversal structure function, $\langle(\Delta_r u_+)^{2p}\rangle_T^{1/p}$, is defined following (1.1) with $\boldsymbol{i}$ replaced by a unit vector $\boldsymbol{j}$ in the spanwise direction.

Figure 8($a$) presents both the fourth-order longitudinal and transversal structure functions for a turbulent boundary layer. The results show that the transversal structure function, $\langle(\Delta_r u_+)^4\rangle_T^{1/2}$, also appears to exhibit a log law for the ECR scales, albeit with a sharper slope (higher $D_p$) compared to its longitudinal counterpart. Similar trends have also been reported by Lee & Moser (2015) and Chandran *et al.* (2017) who examined the streamwise velocity component in the transversal and longitudinal directions. Their results are presented at a comparable $Re$ in wall-bounded turbulence but used the $u$ spectrogram as a diagnostic instead of structure functions to extract

the scaling behaviour of the ECR scales (see Davidson *et al.* 2006). However, based on predictions from the attached eddy model, scaling of both the longitudinal and transversal directions should be equivalent for wall turbulence at high *Re*. Databases to confirm this directly are still unavailable. Nevertheless, once the transversal and longitudinal structure functions are plotted in an ESS inspired form (see figure 8*b*), even at $Re_\tau = O(10^3)$, we observe good agreement between the two for the ECR scales following (3.1). This further highlights that (3.1) is a more robust diagnostic to seek the scaling of the ECR scales.

## 5. Concluding remarks

This work presents evidence of further reaching universality for the ECR scales in wall turbulence by utilising the extended self-similarity hypothesis, i.e. the relative scaling of velocity structure functions. First, the expected scaling for the ratios between velocity structure functions is outlined based on the previously reported log-law scaling for the ECR scales in high Reynolds number boundary layers (Davidson *et al.* 2006; de Silva *et al.* 2015). These predictions are then examined using a range of wall turbulence databases, which span a wide range of Reynolds numbers and flow geometries. The results reveal that the scaling behaviour for the ECR scales extends over a much larger range of scales ($r \gtrsim z$), leading to more precise measurements of the scaling exponents. Further, it is evident that these quantitative measures can now be confidently estimated from databases at much lower Reynolds numbers and over a much larger wall-normal extent than previously thought possible.

Our results also exhibit better universality for the ECR scales across different flow geometries, which before had been claimed to differ, particularly at low/modest Reynolds numbers. This universality for the ECR scales also appears to extend to the transversal streamwise structure function once plotted in ESS form. The latter is in support of the attached eddy model, which predicts equal scaling for both the longitudinal and transversal structure function at sufficiently high Reynolds numbers. A crucial next step would be to show the connection between the universal coefficients $D_n/D_1$ and the universal intermittency exponents $\xi_n$ through some matching conditions between ECR and ISR, but this will be a challenging task.

## Acknowledgements

REFERENCES

DEL ALAMO, J. C., JIMÉNEZ, J., ZANDONADE, P. & MOSER, R. D. 2004 Scaling of the energy spectra of turbulent channels. *J. Fluid Mech.* **500**, 135–144.

ARNEODO, A., BAUDET, C., BELIN, F., BENZI, R., CASTAING, B., CHABAUD, B., CHAVARRIA, R., CILIBERTO, S., CAMUSSI, R., CHILLA, F. *et al.* 1996 Structure functions in turbulence, in various flow configurations, at Reynolds number between 30 and 5000, using extended self-similarity. *Europhys. Lett.* **34**, 411.

ATKINSON, C., BUCHMANN, N. A. & SORIA, J. 2014 An experimental investigation of turbulent convection velocities in a turbulent boundary layer. *Flow Turbul. Combust.* **94**, 1–17.

BELIN, F., TABELING, P. & WILLAIME, H. 1996 Exponents of the structure function in a low temperature helium experiment. *Physica* D **93**, 52.

BENZI, R., CILIBERTO, S., BAUDET, C. & RUIZ-CHAVARRIA, G. 1995 On the scaling of three-dimensional homogeneous and isotropic turbulence. *Physica* D **80**, 385–398.

BENZI, R., CILIBERTO, S., TRIPICCIONE, R., BAUDET, C., MASSAIOLI, F. & SUCCI, S. 1993 Extended self-similarity in turbulent flows. *Phys. Rev.* E **48**, R29–R32.

CHANDRAN, D., BAIDYA, R., MONTY, J. & MARUSIC, I. 2017 Two-dimensional energy spectra in high Reynolds number turbulent boundary layers. *J. Fluid Mech.* (to appear).

CHUNG, D., MARUSIC, I., MONTY, J. P., VALLIKIVI, M. & SMITS, A. J. 2015 On the universality of inertial energy in the log layer of turbulent boundary layer and pipe flows. *Exp. Fluids* **56** (7), 1–10.

CHUNG, D. & MCKEON, B. J. 2010 Large-eddy simulation of large-scale structures in long channel flow. *J. Fluid Mech.* **661**, 341–364.

DAVIDSON, P. A., NICKELS, T. B. & KROGSTAD, P.-Å. 2006 The logarithmic structure function law in wall-layer turbulence. *J. Fluid Mech.* **550**, 51–60.

DEL ALAMO, J. C. & JIMÉNEZ, J. 2009 Estimation of turbulent convection velocities and corrections to Taylor's approximation. *J. Fluid Mech.* **640**, 5–26.

DENNIS, D. J. C. & NICKELS, T. B. 2008 On the limitations of Taylor's hypothesis in constructing long structures in a turbulent boundary layer. *J. Fluid Mech.* **614**, 197–206.

FRISCH, U. 1995 *Turbulence: The Legacy of AN Kolmogorov*. Cambridge University Press.

GROSSMANN, S., LOHSE, D. & REEH, A. 1997a Application of extended self similarity in turbulence. *Phys. Rev.* E **56**, 5473.

GROSSMANN, S., LOHSE, D. & REEH, A. 1997b Different intermittency for longitudinal and transversal turbulent fluctuations. *Phys. Fluids* **9**, 3817–3825.

HUISMAN, S. G., LOHSE, D. & SUN, C. 2013 Statistics of turbulent fluctuations in counter-rotating Taylor–Couette flows. *Phys. Rev.* E **88**, 063001.

HUTCHINS, N., NICKELS, T. B., MARUSIC, I. & CHONG, M. S. 2009 Hot-wire spatial resolution issues in wall-bounded turbulence. *J. Fluid Mech.* **635**, 103–136.

JACOB, B., BIFERALE, L., IUSO, G. & CASCIOLA, C. M. 2004 Anisotropic fluctuations in turbulent shear flows. *Phys. Fluids* **16** (11), 4135–4142.

JIMÉNEZ, J. 2012 Cascades in wall-bounded turbulence. *Annu. Rev. Fluid Mech.* **44**, 27–45.

KUNKEL, G. J. & MARUSIC, I. 2006 Study of the near-wall-turbulent region of the high-Reynolds number boundary layer using an atmospheric flow. *J. Fluid Mech.* **548**, 375–402.

KURIEN, S., LVOV, V. S., PROCACCIA, I. & SREENIVASAN, K. R. 2000 Scaling structure of the velocity statistics in atmospheric boundary layers. *Phys. Rev.* E **61** (1), 407.

LEE, M. & MOSER, R. D. 2015 Direct numerical simulation of turbulent channel flow up to $Re_\tau = 5200$. *J. Fluid Mech.* **774**, 395–415.

MARUSIC, I., MONTY, J. P., HULTMARK, M. & SMITS, A. J. 2013 On the logarithmic region in wall turbulence. *J. Fluid Mech.* **716**, R3.

MENEVEAU, C. & MARUSIC, I. 2013 Generalized logarithmic law for high-order moments in turbulent boundary layers. *J. Fluid Mech.* **719**, R1.

MENEVEAU, C. & SREENIVASAN, K. R. 1987 Simple multifractal cascade model for fully developed turbulence. *Phys. Rev. Lett.* **59** (13), 1424.

MONTY, J. P., HUTCHINS, N., NG, H. C. H., MARUSIC, I. & CHONG, M. S. 2009 A comparison of turbulent pipe, channel and boundary layer flows. *J. Fluid Mech.* **632**, 431–442.

NG, H. C. H., MONTY, J. P., HUTCHINS, N., CHONG, M. S. & MARUSIC, I. 2011 Comparison of turbulent channel and pipe flows with varying Reynolds number. *Exp. Fluids* **51** (5), 1261–1281.

NICKELS, T. B., MARUSIC, I., HAFEZ, S. & CHONG, M. S. 2005 Evidence of the $k^{-1}$ law in a high-Reynolds-number Turbulent Boundary Layer. *Phys. Rev. Lett.* **95** (7), 074501.

PERRY, A. E., HENBEST, S. M. & CHONG, M. 1986 A theoretical and experimental study of wall turbulence. *J. Fluid Mech.* **165**, 163–199.

POPE, S. B. 2000 *Turbulent Flows*. Cambridge University Press.

SHE, Z. S. & LEVEQUE, E. 1994 Universal scaling law in fully developed turbulence. *Phys. Rev. Lett.* **72**, 1424.

SILLERO, J. A., JIMÉNEZ, J. & MOSER, R. D. 2013 One-point statistics for turbulent wall-bounded flows at Reynolds numbers up to $\delta^+ = 2000$. *Phys. Fluids* **25** (10), 105102.

DE SILVA, C. M., MARUSIC, I., WOODCOCK, J. D. & MENEVEAU, C. 2015 Scaling of second-and higher-order structure functions in turbulent boundary layers. *J. Fluid Mech.* **769**, 654–686.

SMITS, A. J., MCKEON, B. J. & MARUSIC, I. 2011 High-Reynolds number wall turbulence. *Annu. Rev. Fluid Mech.* **43**, 353–375.

TOWNSEND, A. A. 1976 *The Structure of Turbulent Shear Flow*, 2nd edn. Cambridge University Press.

VAN DE WATER, W. & HERWEIJER, J. A. 1999 High-order structure functions of turbulence. *J. Fluid Mech.* **387**, 3–37.

YANG, X. I. A., MARUSIC, I. & MENEVEAU, C. 2016a Moment generating functions and scaling laws in the inertial layer of turbulent wall-bounded flows. *J. Fluid Mech.* **791**, R2.

YANG, X. I. A., MENEVEAU, C., MARUSIC, I. & BIFERALE, L. 2016b Extended self-similarity in moment-generating-functions in wall-bounded turbulence at high Reynolds number. *Phys. Rev. Fluids* **1** (4), 044405.